Journal Pre-proof

Using molecular dynamics to predict the solidus and liquidus of mixed oxides (Th,U)O2, (Th,Pu)O2 and (Pu,U)O2,

C.O.T. Galvin, P.A. Burr, M.W.D. Cooper, P.C.M. Fossati, R.W. Grimes

PII: S0022-3115(19)31459-X

DOI: https://doi.org/10.1016/j.jnucmat.2020.152127

Reference: NUMA 152127

To appear in: *Journal of Nuclear Materials*

Received Date: 11 November 2019

Revised Date: 18 March 2020

Accepted Date: 18 March 2020

Please cite this article as: C.O.T. Galvin, P.A. Burr, M.W.D. Cooper, P.C.M. Fossati, R.W. Grimes, Using molecular dynamics to predict the solidus and liquidus of mixed oxides (Th,U)O2, (Th,Pu)O2 and (Pu,U)O2, *Journal of Nuclear Materials* (2020), doi: https://doi.org/10.1016/j.jnucmat.2020.152127.

Using Molecular Dynamics to Predict the Solidus and Liquidus of Mixed Oxides $(Th,U)O_2$, $(Th,Pu)O_2$ and $(Pu,U)O_2$

C. O. T. Galvin[a], P. A. Burr[a], M. W. D. Cooper[b], P. C. M. Fossati[c], R. W. Grimes[d]

[a]*School of Mechanical and Manufacturing Engineering, University of New South Wales, Kensington, 2052, NSW, Australia*
[b]*Materials Science and Technology Division, Los Alamos National Laboratory, P.O. Box 1663, Los Alamos, New Mexico 87545, USA*
[c]*DEN–Service de Corrosion et du Comportement des Matériaux dans leur Environnement (SCCME), CEA Saclay, Université Paris Saclay, F-91191 Gif-sur-Yvette, France*
[d]*Department of Materials, Imperial College London, London, SW7 2AZ, UK*

Abstract

Molecular dynamics (MD) was used to establish a mechanistic basis for the experimentally observed reduction in liquidus and solidus temperatures below the melting point of the end-members for the mixed oxides $(Th,U)O_2$, $(Th,Pu)O_2$ and $(Pu,U)O_2$. This dip is found at ~5% additions of the oxide with higher melting point to the oxide with the lower melting point. There are many causes suggested for the dip; here the distribution of the cation Frenkel energy for the mixed oxides caused by the local environment is proposed as a contributor. Furthermore, a variant of the moving interface method which yields information on the position of the solidus and liquidus boundaries, is used to predict the phase diagrams of these systems.

1. Introduction

It is necessary to have a detailed knowledge of the melting behaviour of actinide oxides in order to understand their thermodynamic and structural stability. In terms of nuclear fuel, the melting temperature is an input parameter in performance design and safety. For example, it determines the maximum allowed centerline temperature and therefore the maximum diameter fuel-pin design. It is also an important property when predicting nuclear fuel evolution under accident conditions. Moreover, knowledge of how melting behaviour varies as a function of composition is necessary in the sintering process to optimise the fabrication of chemically

Email address: r.grimes@imperial.ac.uk (R. W. Grimes)

homogeneous mixed oxide (MOX) fuel pellets. Nevertheless, for oxide fuels, there is some controversy surrounding melting point values. This is especially true for PuO_2. Measurements from Kato *et al.* [1] and De Bruycker *et al.* [2, 3] suggest much higher values than were previously assumed. The principal issue has been the chemical interaction between the sample and the crucible, which can result in lower phase transition temperatures [1, 4]. Similar temperature depreciation effects could have a great influence on the solidus and liquidus of PuO_2-based MOX fuels and work has been conducted to redefine Pu-based MOX phase diagrams [5, 6].

Binary MOX systems are known to exhibit solid solubility across their whole compositional range [7, 8]. Initially, this had led to the belief that mixed oxides exhibit ideal solution behaviour, where the predicted phase coexistence domain, bounded by the solidus and liquidus, has a simple lenticular shape. However, a significant body of work has been conducted in dealing with the U-Pu oxide systems which has led to efforts on non-ideal mixed oxide description [9–12]. For example, using the extrapolation of binary oxides, Besmann and Lindemer developed a thermochemical model in the 80's [13–15] which reproduced the available experimental data on $UO_{2\pm x}$, PuO_{2-x} and $(U,Pu)O_{2\pm x}$. Subsequent thermodynamic work also takes into account the possibility of congruent melting at non-stoichiometric oxygen ratios [16, 17], and a number of subsequent publications consider the effect of non-ideal mixing behaviour in mixed oxides [6, 18–21].

Taking as an example ThO_2, which has the highest melting temperature of all actinide oxides [22], if the mixed $(Th,U)O_2$ and $(Th,Pu)O_2$ systems displayed ideal mixing, then all points on the liquidus and solidus would be lower than the melting point of ThO_2. Therefore, adding any amount of ThO_2 to other actinide oxides would increase the melting point. Here we find that this is not necessarily the case, and that small additions of ThO_2 to either UO_2 or PuO_2 lead to a reduction of the solidus and liquidus temperatures.

The concept of MOX phase coexistence domains being bounded by a simple lenticular domain is challenged in some publications [6, 19–21, 23, 24]. This would mean that the mixed oxides do not behave in an ideal manner. It can, however, be difficult to control environments

and unambiguously deconvolute mechanistic behaviour from experiment. Molecular dynamics (MD) simulations are therefore useful in predicting possible mechanisms for non-ideal melting point behaviour without experimental constraints or artefacts, that is, to complement experiment. Using the moving interface method, we have previously calculated congruent melting points over a range of compositions for $(Th,U)O_2$ and $(Th,Pu)O_2$ binary MOX compositions [25] and here extend to $(Pu,U)O_2$. Predicted non-lenticular shapes suggest that these systems may not be ideal. However, these previous calculations were not able to determine if the melting points correspond to the liquidus, the solidus or somewhere in the region between these two due to an inherent limitation of the moving interface method. Here, a new modified moving interface method (described in [26]) is used to identify points on the solidus and liquidus for $(Th,U)O_2$, $(Th,Pu)O_2$ and $(Pu,U)O_2$ MOX systems and therefore leads to a more complete prediction of binary phase diagrams.

2. Methodology

2.1. Model Development

On the assumption that these binary solid solutions are ideal solutions, such that there are no volume or enthalpy changes on mixing when they form, it is possible to calculate the liquidus and solidus, given the melting points and enthalpies of fusion of the two end-members, by solving the following set of equations [27];

$$\frac{S_\alpha}{L_\alpha} = \exp\left[\frac{\Delta H_{m\alpha}}{R}\left(\frac{1}{T_{m\alpha}} - \frac{1}{T}\right)\right] \tag{1}$$

$$\frac{S_\beta}{L_\beta} = \exp\left[\frac{\Delta H_{m\beta}}{R}\left(\frac{1}{T_{m\beta}} - \frac{1}{T}\right)\right] \tag{2}$$

where T_m is the melting temperatures of the end-members (α and β), R is the ideal gas constant (8.3143 $\frac{\mathrm{J}}{\mathrm{mol}}$ K) and ΔH_m are the enthalpies of fusion of the two end-members (α and

β). S_α/L_α is the ratio between the mole fractions in the solidus and liquidus for one end-member at temperature T and S_β/L_β the other end-member. The actual positions of the solidus and liquidus may then be calculated by applying the further constraint that the sum of the mole fractions of the two components must equal one (i.e. equations 3 and 4).

$$S_\alpha + S_\beta = 1 \tag{3}$$

$$L_\alpha + L_\beta = 1 \tag{4}$$

If the solution is not ideal, a simple lenticular shape of the solidus and liquidus cannot be assumed and a new method is needed to calculate solidus and liquidus. To this end it is important to understand the moving interface method (also known as the phase coexistence method) for predicting melting temperatures [28]. For the moving interface method, simulation cells contain two pre-equilibrated regions, a solid region and a liquid region, and two solid-liquid interfaces (see figure 1). By monitoring the position of the interfaces over the course of an MD run at a desired temperature (i.e. equilibrating the whole system in an NPT ensemble at a chosen temperature) it is possible to determine if the temperature of the system is above or below the melting point predicted by the potential model. The growth of either the solid or liquid phase (through movement of the interface) establishes if the temperature chosen for the MD calculation is above or below the melting point.

The modified moving interface method is very similar to the conventional moving interface method, except that the composition is adjusted rather than temperature. So, instead of having one side of the system as a solid regime and the other in a liquid regime, sharing the same composition, each side of the interface is given a different composition. The method will be referred to as the compositional moving interface (CMI) method and is summarised below with respect to the schematic binary phase diagram in figure 2 a.

1. Choose a temperature, T, (figure 2b), that lies between the melting points of the end-members.
2. Create a liquid structure at that temperature (figure 2c) for end-member A.
3. Create a solid structure at an arbitrary composition that is estimated not to be in the liquid phase at this temperature (figure 2c, in this case it is the pure B end-member).
4. Combine the two structures to obtain a single system with the two distinct compositions at opposite ends of the simulation box (figure 2d).
5. Run an MD calculation at the chosen temperature. With these compositions, the two phases can coexist during the MD run and the interface should not move significantly (figure 2d).
6. The MD calculation procedure is repeated iteratively with the composition of the liquid region held fixed (pure A) but with a modified composition for the solid region (by increasing the proportion of A). Under the conditions illustrated in figure 2e, the liquid and solid phases can co-exist at temperature T and again the interface should not move significantly.
7. Upon modifying the composition of the solid further (figure 2f), the system energy is high and only the liquid phase can exist and therefore, the liquid side of the system will grow and the whole system will become liquid. This identifies a point on the liquidus.
8. To calculate a point on the solidus the converse simulation must be carried out, that is, the composition of the solid is kept constant and the composition of the liquid region is changed until the whole system becomes solid during the MD run.

In these liquidus simulations, the liquid is acting as an initiator of the dissolution process for a solid that should be in the liquid state. Similarly for the solidus simulations, the solid is offering nucleation for crystallisation for a liquid that should be in the solid state. Both of these are essentially kinetic processes. On significantly shorter timescales for some compositions the solid may exhibit some dissolution into the liquid. This is because it reduces the total system energy because the liquid is not in equilibrium with the solid, and for sufficiently long simulations the interface can be seen to move a little into the solid, but the timescales are distinctly

different to these melting or crystallisation process.

2.2. Computation Methodology

MD simulations were carried out using the LAMMPS code [29] and the interatomic forces were described using the CRG potential [30]. The CRG potential accurately reproduces the experimentally determined melting points of UO_2 and ThO_2, while the PuO_2 melting point is within the bounds of experimental data (there is a large range of experimentally reported melting temperatures) [31]. The CRG allows the calculation of mixed oxides and is successful at predicting relevant thermophysical properties [25, 30, 32–36]. Coulombic interactions were calculated using an Ewald summation. For all simulations reported here an NPT ensemble was implemented with zero external pressure using a Nosé-Hoover barostat and thermostat with relaxation times of 0.5 ps and 0.1 ps respectively.

The conventional moving interface method was used to calculate the melting points of $(Pu,U)O_2$, similarly to previous work on $(U,Th)O_2$ and $(Pu,Th)O_2$ [25]. The system consisted of a $45 \times 5 \times 5$ supercell (13,500 atoms), in the cubic fluorite structure with Pu^{4+} and U^{4+} cations randomly distributed across the cation sites. To create the liquid and solid region within the supercell the whole system was first equilibrated at the test temperature, 3000 K, at 0 GPa. The simulation box was then split into two equal regions, a 'solid' region and a 'liquid' region, both with the same composition. Then a liquid state was produced by inducing atomic disorder in the liquid region by heating that region to 5000 K, at 0 GPa, and then equilibrating the liquid region at 4000 K. This resulted in an atomic configuration consistent with a liquid phase at 4000 K. The other region remained a solid fluorite crystal structure at 3000 K. This results in a small energy difference due to the different temperature and the phase change between the atoms in the liquid and solid phases. The entire system was then relaxed under NPT with box relaxation of the barostat allowed in the x-direction (normal to the interface) only to avoid stresses in the solid region. The interface was monitored at different temperatures to determine when the system melted.

For each CMI structure two $25 \times 5 \times 5$ supercells of different compositions were combined to create a $50 \times 5 \times 5$ supercell. The solid regions of $(U,Th)O_2$, $(Pu,Th)O_2$ and $(Pu,U)O_2$ CMI structures for liquidus calculations were composed of the MOX composition under investigation while the liquid region consisted of the end-member with the lower melting temperature (e.g. the solid region of $(U,Th)O_2$ consisted of $(U,Th)O_2$ and the liquid region of UO_2). For solidus calculations of $(U,Th)O_2$, $(Pu,Th)O_2$ and $(Pu,U)O_2$ the liquid regions were composed with the MOX composition and the solid regions were composed of the end-member with the higher melting temperature (e.g the liquid region of $(U,Th)O_2$ consisted of $(U,Th)O_2$ and the solid region of ThO_2). Simulation systems containing a solid and liquid region were created using the same procedure as outlined above. A 3 ns MD run was then implemented at a specific temperature to determine whether the system was in a solid, a liquid or a solid-liquid state.

Isolated cation Frenkel defect energies for four $(Pu,Th)O_2$ compositions, and their end-members PuO_2 and ThO_2, were calculated as reported previously [34] in a $10 \times 10 \times 10$ supercell. Cation vacancies are created by removing each cation from lattice sites one at a time in separate simulations. For the case of $(Pu_{95},Th_5)O_2$ this is 3800 Pu vacancy simulations and 200 Th vacancy simulations. Moreover, 8000 interstitial defect simulations were created by placing 4000 Pu cations and 4000 Th cations at interstitial sites[1]. Finally, Frenkel energies are determined by combining the energies of all vacancy-interstitial pairs (1.6×10^7 combinations).

3. Results and Discussion

3.1. Ideal solidus and liquidus lines and melting temperatures using the moving interface method

As described in section 2, for ideal solutions, the solidus and liquidus of the binary phase diagram are solely defined by the enthalpies of fusion and the melting temperatures of the two end-members. The ideal solidus-liquidus curves in figures 3, 4 and 5 were thus created using equations 1-4 with the melting points and enthalpies of fusion of PuO_2, ThO_2 and UO_2 from experimental literature [1, 3, 37–40] (dashed black lines) and from MD simulations [25] (dashed solid red and blue lines). This approach assumes that the heat capacity is the same

[1] The vacancy and interstitial defect energy plots are given in the supplementary material section.

for both solid and liquid phases close to melting and the configurational entropy is the only differentiating contribution to the Gibbs free energy.

Results from the conventional moving interface simulations (green triangle data points in figures 3b, 4b and 5b) sometimes indicate deviation from ideal mixture predictions. Specifically, adding ~5 at% of ThO_2 to PuO_2 or UO_2 lowers the melting temperature compared to the pure majority end-member and corresponds to a minimum in the phase diagram (see figures 3 and 4). This minimum was also observed experimentally by Böhler *et al.* [21] and by Latta *et al.* [41] in $(Pu,Th)O_2$ and $(U,Th)O_2$, respectively. These minima indicate a deviation from an ideal binary solution and thus, the systems cannot be represented by an ideal solution model, or even regular behaviour. For the $(Pu,U)O_2$ system De Bruycker *et al.* [5] predicted a minimum melting point at ~50-80 at% PuO_2. Similarly, using the same technique, Böhler *et al.* [19] suggest the presence of a minimum at ~40-70 at% PuO_2. However, this is not supported by older experimental data [1, 40, 42] and is not seen in the simulations reported here. In those experiments it is suggested reaction of PuO_2 samples with the container and/or changes in the O/M ratio at high temperature affected the results. The formation of a stable oxygen gas phase at high temperatures for the PuO_2-rich part of the pseudo-binary $(Pu,U)O_2$ phase diagram must be considered [5]. According to Guéneau *et al.* [6] plutonium dioxide melts congruently at a slightly hypo-stoichiometric composition ($PuO_{1.96}$). In a reducing environment PuO_2 would lose oxygen before melting. Therefore, for an (O/M = 2.00), the melting of plutonium dioxide involves the oxygen gas phase (see CALPHAD predictions on figure 5a). The effect of the O/M ratio on the melting temperature should be considered in the ternary U-Pu-O phase diagram rather than the pseudo-binary $(Pu,U)O_2$ [6]. Oxygen non-stoichiometry largely influences the material behaviour in the U-Pu-O ternary system, because of the relatively easy valence shifts of U atoms from +4 to +5 and +6, and of Pu atoms from +4 to +3. The behaviour is essentially different in the $(Pu,Th)O_2$ and $(U,Th)O_2$ systems, because of the very stable +4 valency state of Th, which stabilises the stoichiometric dioxide phase (O/M = 2.00) throughout the pseudo-binary plane. This could explain why the MD simulations fail in reproducing the experimentally observed trend in the $(Pu,U)O_2$ system, whereas they successfully confirm that the investigated systems deviate from an ideal behaviour. Nevertheless, the current simulations are not incon-

sistent with a small minimum at 95 at% PuO_2 for the $(Pu,U)O_2$ system.

There are a number of suggestions put forward to explain why minima are observed in the experimental literature. One argument is that there is a change in stoichiometry, however, the melting point calculations reported here are for stoichiometric compositions and minima are still predicted. Böhler *et al.* [21] mention that factors such as lattice strain caused by a difference in ionic radii of Pu^{4+} and Th^{4+} can also be responsible for a minimum. The minimum observed in the MD simulation results could therefore be a consequence of the lattice parameter mismatch between the end-members as also mentioned in previous simulation publications [32–34].

Cations in MOX will exhibit different local environments due to different interatomic separations. These deviate from the average dictated by the lattice parameter of the bulk system. For instance, in $(Th,Pu)O_2$ a Pu atom is surrounded by 12 nearest neighbour cations, which could all be Th atoms, or they could be 11 Th and one Pu, or 10 Th and two Pu, and so on leading to many possible configurations. This leads to many slightly different vacancy and interstitial defect formation energies, which combine to generate different Frenkel formation energies. Figure 6 shows the distribution of Frenkel formation energies for 25%, 50% and 75% and 95% addition of Pu to ThO_2. For the end-members (PuO_2 and ThO_2) the energy of a (dilute) Frenkel pair has a singular and well defined energy, as all sites are identical in the undoped fluorite crystal. However, upon mixing, the spread in energy becomes quite significant. Interestingly this spread has well-defined peaks in the Frenkel energy distribution, as seen for other solid solutions [32–34], a consequence of the number of permutations of the local environment (1^{st} nearest neighbour shell). As a result, even a small amount of Th in solid solution (e.g. 5%), leads to the creation of a significant number of Frenkel pairs with lower formation energy than that found in undoped PuO_2 (shaded purple area in figure 6). Moreover, by examining the median values (shown as coloured dashed lines on figure 6) it is clear the median value (12.3 eV) of the isolated Frenkel energy for 5% Th in solid solution with PuO_2 is lower than the isolated Frenkel energy for PuO_2 (12.47 eV). That is, more than half of the Frenkel pair configurations have lower energy than that of the pure PuO_2 system at this composition. Then, as more solute

is added, the average effect on the crystal takes effect and the average Frenkel energy increases. The presence of a majority of lower energy Frenkel defects means that cation Frenkel disorder will increase as temperature rises more quickly in the 5% ThO_2 MOX compared to the end-members. This more rapid increase in cation defect concentration will act to lower the melting temperature of the 5% ThO_2 MOX compositions but is not the only factor to consider. The defect concentration effect is a second order effect that is competing with the average increase in bond strength as a consequence of increasing amounts of the higher melting point material (captured in the model of ideal and regular solutions). This is manifest as a gradual shift to higher energies of all Frenkel pair configurations, clear at higher Th content in figure 6.

The rationalisation of the minimum in melting point with composition, observed both experimentally and computationally, is an illustration that these systems do not behave in an ideal manner. Therefore, the previous assumption that the binary MOX systems exhibits a close ideal behaviour and have a lenticular shape on the phase diagram is not valid.

3.2. Compositional Moving Interface

It is not clear whether the unary melting points calculated using the (conventional) moving interface method, reported by Ghosh *et al.* [25] (figures 3b, 4b, 7 and 8) and calculated here (figures 5b and 9), correspond to the solidus, the liquidus or somewhere in between.

The phase diagrams proposed on the basis of the CMI MD points with the corresponding MD melting points using the moving interface method are presented in figures 7, 8 and 9. In each figure, the red and blue bars correspond to the range of compositions where the liquidus and solidus are calculated using the CMI method. The unary melting temperatures calculated using the conventional moving interface method (green data points) are also shown on these plots for comparison with the solidus and liquidus points. There is an excellent agreement between the two methods with the CMI method giving new information about the position of the solidus and liquidus, and avoiding assumptions of ideal behaviour of MOX. In all cases the green points sit within the CMI liquidus and solidus bounds suggesting that the unary method

predicts values within the two phase coexistence region.

The CMI predictions are consistent with the MOX solid solution exhibiting deviations from ideal, or even regular, behaviour, with a widening of the solid/liquid coexistence region at high Pu in $(Th,Pu)O_2$ and high U in $(Pu,U)O_2$.

4. Conclusions

These simulations are consistent with the premise that binary MOX systems cannot be approximated as ideal mixtures. Further, the experimental observations of a dip in the solidus and liquidus for binary MOX systems are seen in these MD predictions. There are a number of suggested causes for these minima, one of which is the lattice mismatch of the end member thereby influencing the Frenkel formation energies of the MOX (made of the composition located at the minimum) compared to the end-members. That is, cation Frenkel defects form at lower energies than the end-members suggesting they contribute to melting at lower temperatures. Of course there are a number of other factors that could cause experimentally observed deviation from assumed ideal behaviour, such as non-stoichiometry. Nevertheless, despite our model not considering non-stoichiometry it is still able to predict non-ideal behaviour.

A new CMI method using MD was then applied to determine if it could be used to predict solidus and liquidus curves for $(Th,Pu)O_2$, $(Th,U)O_2$ and $(U,Pu)O_2$. These are in agreement with the unitary melting points (green data points) predicted using the moving interface method but provide additional information about the position of the solidus and liquidus curves. The CMI method shows it is possible to use MD to establish the bounds of the solidus and liquidus for a binary oxide system. With the statistics available with the current set of calculations, the CMI method does not clearly identify a minimum as suggested by experiments [19–21] and the MD melting points. However, there is a clear deviation from the ideal lenticular shape shown by the CMI method and the results are not inconsistent with minima. This is the first attempt at such calculations and refinements of the method are currently being considered.

This work highlights the use of MD to predict experimental observations and attempt to shed light on fundamental mechanisms governing this behaviour. Furthermore, it can be expanded using a newly developed method to predict binary phase diagrams of MOX systems.

Acknowledgements

This work was undertaken with the assistance of resources and services from the National Computational Infrastructure (NCI), which is supported by the Australian Government, and the Multi-modal Australian ScienceS Imaging and Visualisation Environment (MASSIVE). This research was also supported by resources provided by the Pawsey Supercomputing Centre with funding from the Australian Government and the Government of Western Australia. Computational resources were also provided be the Imperial College High Performance Computing Service.

[1] M. Kato, K. Morimoto, H. Sugata, K. Konashi, M. Kashimura, and T. Abe. Solidus and liquidus temperatures in the UO_2–PuO_2 system. *Journal of Nuclear Materials*, 373(1-3):237–245, feb 2008.

[2] F. De Bruycker, K. Boboridis, D. Manara, P. Pöml, M. Rini, and R. J.M. Konings. Reassessing the melting temperature of PuO_2. *Materials Today*, 13(11):52–55, nov 2010.

[3] F. De Bruycker, K. Boboridis, P. Pöml, R. Eloirdi, R. J. M. Konings, and D. Manara. The melting behaviour of plutonium dioxide: A laser-heating study. *Journal of Nuclear Materials*, 416(1-2):166–172, 2011.

[4] M. Kato, K. Morimoto, H. Sugata, K. Konashi, M. Kashimura, and T. Abe. Solidus and liquidus of plutonium and uranium mixed oxide. *Journal of Alloys and Compounds*, 452(1):48–53, mar 2008.

[5] F. De Bruycker, K. Boboridis, R. J. M. Konings, M. Rini, R. Eloirdi, C. Guéneau, N. Dupin, and D. Manara. On the melting behaviour of uranium/plutonium mixed dioxides with high-Pu content: A laser heating study. *Journal of Nuclear Materials*, 419(1-3):186–193, 2011.

[6] C. Guéneau, N. Dupin, B. Sundman, C. Martial, J. Dumas, S. Gossé, S. Chatain, F. De Bruycker, D. Manara, and R. J. M. Konings. Thermodynamic modelling of advanced oxide and carbide nuclear fuels : Description of the U – Pu – O – C systems. *Journal of Nuclear Materials*, 419(1-3):145–167, 2011.

[7] O. S. Vălu, O. Beneš, R. J. M. Konings, and H. Hein. The high temperature heat capacity of the (Th,Pu)O_2 system. *The Journal of Chemical Thermodynamics*, 68(5):122–127, jan 2014.

[8] S. O. Vălu, O. Beneš, D. Manara, R. J.M. Konings, M. W. D. Cooper, R. W. Grimes, and C. Guéneau. The high-temperature heat capacity of the (Th,U)O_2 and (U,Pu)O_2 solid solutions. *Journal of Nuclear Materials*, 484:1–6, feb 2017.

[9] P. E. Blackburn and C. E. Johnson *Thermodynamics of nuclear materials 1974 : proceedings of a Symposium on the Thermodynamics of Nuclear Materials,pp 17-33,1974*.

[10] P. E. Blackburn and C. E. Johnson. Chemical modelling of uranium, plutonium and oxygen redistribution in oxide fuels by vapour transport and diffusion. Technical report, IAEA Symposium on Thermodynamics of Nuclear Materials, 1974.

[11] J. Edwards, R. N. Wood, and G. R. Chilton. Oxygen potentials of uranium-plutonium oxides in the near stoichiometric region. *Journal of Nuclear Materials*, 130:505–512, feb 1985.

[12] H. A. Wriedt. The O-Pu (Oxygen-Plutonium) system. *Bulletin of Alloy Phase Diagrams*, 11(2):184–202, apr 1990.

[13] T. M. Besmann and T. B. Lindemer. Chemical thermodynamic representations of (PuO_{2-x}) and ($U_{1-z}Pu_zO_w$). *Journal of Nuclear Materials*, 130(C):489–504, feb 1985.

[14] T. B. Lindemer and T. M. Besmann. Chemical thermodynamic representation of ($UO_{2\pm x}$). *Journal of Nuclear Materials*, 130:473–488, feb 1985.

[15] T. M. Besmann and T. B. Lindemer. Improvement in the chemical thermodynamic representation of(PuO_{2-x}) and ($U_{1-z}Pu_zO_w$). *Journal of Nuclear Materials*, 137(3):292–293, feb 1986.

[16] C. Guéneau, C. Chatillon, and B. Sundman. Thermodynamic modelling of the plutonium - oxygen system. 378:257–272, 2008.

[17] M. Kato, S. Nakamichi, K. Takeuchi, and T. Sunaoshi. Measurement of oxygen potential of $(U_{0.8}Pu_{0.2})O_{2\pm x}$ at 1773 and 1873 K, and its analysis based on point defect chemistry. *Calphad*, 35(4):623–626, dec 2011.

[18] D. Manara, R. Böhler, K. Boboridis, L. Capriotti, L. Luzzi, F. De Bruycker, C. Guéneau, and N. Dupin. The melting behaviour of oxide nuclear fuels : effects of the oxygen potential studied by laser heating. 7:505–512, 2012.

[19] R. Böhler, M.J. Welland, D. Prieur, P. Cakir, T. Vitova, T. Pruessmann, I. Pidchenko, C. Hennig, C. Guéneau, R.J.M. Konings, and D. Manara. Recent advances in the study of the UO_2–PuO_2 phase diagram at high temperatures. *Journal of Nuclear Materials*, 448(1-3):330–339, may 2014.

[20] R. Böhler, A. Quaini, L. Capriotti, P. Çakır, O. Beneš, K. Boboridis, A. Guiot, L. Luzzi, R.J.M. Konings, and D. Manara. The solidification behaviour of the UO_2–ThO_2 system in a laser heating study. *Journal of Alloys and Compounds*, 616:5–13, dec 2014.

[21] R. Böhler, P. Çakır, O. Beneš, H. Hein, R. J. M. Konings, and D. Manara. High temperature phase transition of mixed (PuO_2+ThO_2) investigated by laser melting. *The Journal of Chemical Thermodynamics*, 81:245–252, 2015.

[22] F. Cappia, D. Hudry, E. Courtois, A. Janßen, L. Luzzi, R. J. M. Konings, and D. Manara. High-temperature and melting behaviour of nanocrystalline refractory compounds: an experimental approach applied to thorium dioxide. *Materials Research Express*, 1(2):025034, jun 2014.

[23] J. Kim and S. S. Kim. Thermodynamic modeling of the UO_2–ThO_2 phase diagram. *Modelling and Simulation in Materials Science and Engineering*, 24(2):025010, feb 2016.

[24] L. Zhang, A. Shelyug, and A. Navrotsky. Thermochemistry of UO_2 – ThO_2 and UO_2 – ZrO_2 fluorite solid solutions. *The Journal of Chemical Thermodynamics*, 114:48–54, nov 2017.

[25] P. S. Ghosh, N. Kuganathan, C. O. T. Galvin, A. Arya, G. K. Dey, B. K. Dutta, and R. W. Grimes. Melting behavior of (Th,U)O_2 and (Th,Pu)O_2 mixed oxides. *Journal of Nuclear Materials*, 479:112–122, oct 2016.

[26] C. O. T. Galvin, P. A. Burr and R. W. Grimes. An MD Method to Identify the Liquidus and Solidus in a Binary Phase Diagram. *manuscript submitted for publication.*

[27] R. A. Swalin and S. A. Rice. Thermodynamics of Solids. *Physics Today*, 16(1):72–74, jan 1963.

[28] K. Govers, S. Lemehov, M. Hou, and M. Verwerft. Comparison of interatomic potentials for UO_2. *Journal of Nuclear Materials*, 376(1):66–77, may 2008.

[29] S. Plimpton. Fast Parallel Algorithms for Short-Range Molecular Dynamics, 1995.

[30] M. W. D. Cooper, M. J. D. Rushton, and R. W. Grimes. A many-body potential approach to modelling the thermomechanical properties of actinide oxides. *Journal of Physics: Condensed Matter*, 26(10):105401, mar 2014.

[31] C. Guéneau, A. Chartier, and L. Van Brutzel. *Thermodynamic and Thermophysical Properties of the Actinide Oxides*, volume 2. Elsevier, 2012.

[32] M. W. D. Cooper, S. T. Murphy, P. C. M. Fossati, M. J. D. Rushton, and R. W. Grimes. Thermophysical and anion diffusion properties of (U_x,Th_{1-x})O_2. *Proceedings of the Royal Society A: Mathematical, Physical and Engineering Sciences*, 470(2171):20140427–20140427, sep 2014.

[33] M. W. D. Cooper, S. C. Middleburgh, and R. W. Grimes. Modelling the thermal conductivity of (U_x,Th_{1-x})O_2 and (U_x,Pu_{1-x})O_2. *Journal of Nuclear Materials*, 466:29–35, 2015.

[34] C. O. T. Galvin, M. W. D. Cooper, M. J. D. Rushton, and R. W. Grimes. Thermophysical properties and oxygen transport in (Th_x,Pu_{1-x})O_2. *Scientific Reports*, 6(October):36024, oct 2016.

[35] H. Balboa, L. Van Brutzel, A. Chartier, and Y. Le Bouar. Assessment of empirical potential for MOX nuclear fuels and thermomechanical properties. *Journal of Nuclear Materials*, 495:67–77, nov 2017.

[36] H. Nakamura and M. Machida. High-temperature properties of thorium dioxide: A first-principles molecular dynamics study. *Journal of Nuclear Materials*, 478:56–60, sep 2016.

[37] J. Belle. Thorium dioxide: properties and nuclear applications. Technical Report 2-3, USDOE Office of Nuclear Energy, Science and Technology (NE), jan 1984.

[38] K. Bakker, E. H. P. Cordfunke, R. J. M. Konings, and R. P. C. Schram. Critical evaluation of the thermal properties of ThO_2 and $Th_{1-y}U_yO_2$ and a survey of the literature data on $Th_{1-y}Pu_yO_2$. *Journal of Nuclear Materials*, 250(1):1–12, 1997.

[39] L. F. Epstein. Ideal solution behavior and heats of fusion from the UO_2-PuO_2 phase diagram. *Journal of Nuclear Materials*, 22(3):340–349, jun 1967.

[40] M. G. Adamson, E. A. Aitken, and R. W. Caputi. Experimental and thermodynamic evaluation of the melting behavior of irradiated oxide fuels. *Journal of Nuclear Materials*, 130(C):349–365, feb 1985.

[41] R. E. Latta, E. C. Duderstadt, and R. E. Fryxell. Solidus and liquidus temperatures in the UO_2-ThO_2 system. *Journal of Nuclear Materials*, 35(3):347–349, jun 1970.

[42] W. L. Lyon and W. E. Baily. The solid-liquid phase diagram for the UO_2-PuO_2 system. *J. Nucl. Mater.*, 22:332–339, 1967.

[43] W. A. Lambertson, M. H. Mueller, and F. H. Gunzel. Uranium Oxide Phase Equilibrium Systems: IV, UO_2-ThO_2 . *Journal of the American Ceramic Society*, 36(12):397–399, dec 1953.

[44] General Electric. Quarterly report Ceramics research and development operation. Technical report, 1962.

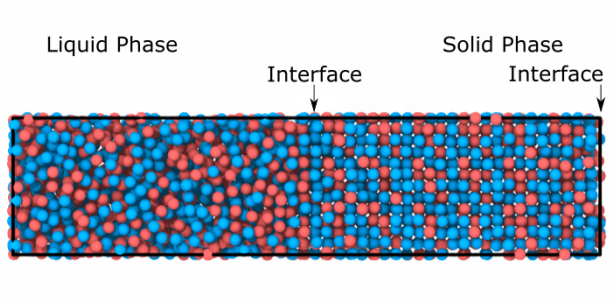

Figure 1: A schematic of the moving interface method where the red and blue colours denote two different atom types.

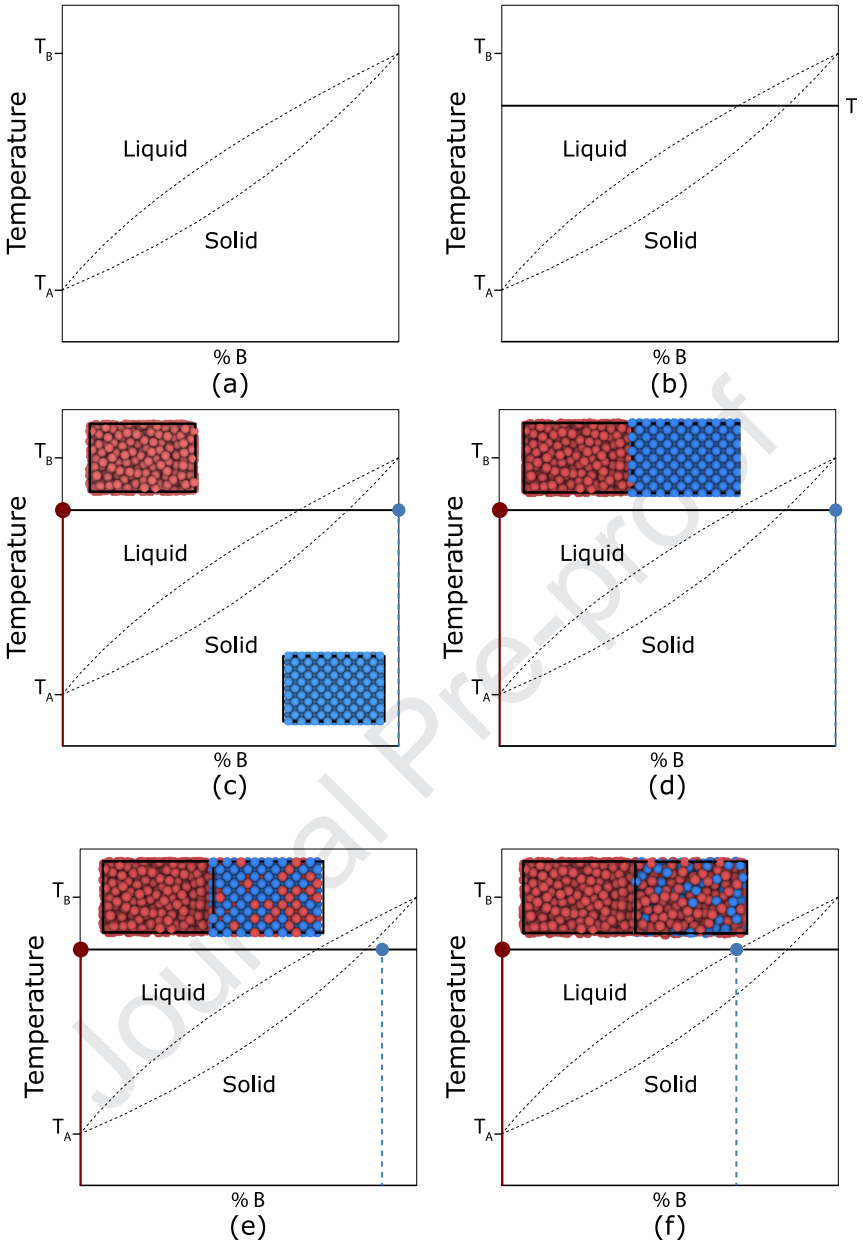

Figure 2: Schematic representing the compositional moving interface (CMI) method as a function of time. (a) represents a typical binary phase diagram for an *A*, *B* system. (b) shows a chosen temperature, *T*, on the binary phase diagram. The points on (c) indicate pure liquid *A* and *B* solid phases at the beginning of the simulation. (d) shows the complete simulation cell and interface. (e) shows a second point representing a different composition of the solid with a greater proportion of *A* that still results in two-phase coexistance. (f) shows a third composition with a yet greater proportion of *A* for which only a liquid phase is thermodynamically stable and thus the solid has melted. The initial composition of the solid region is marked as the liquidus point at that temperature.

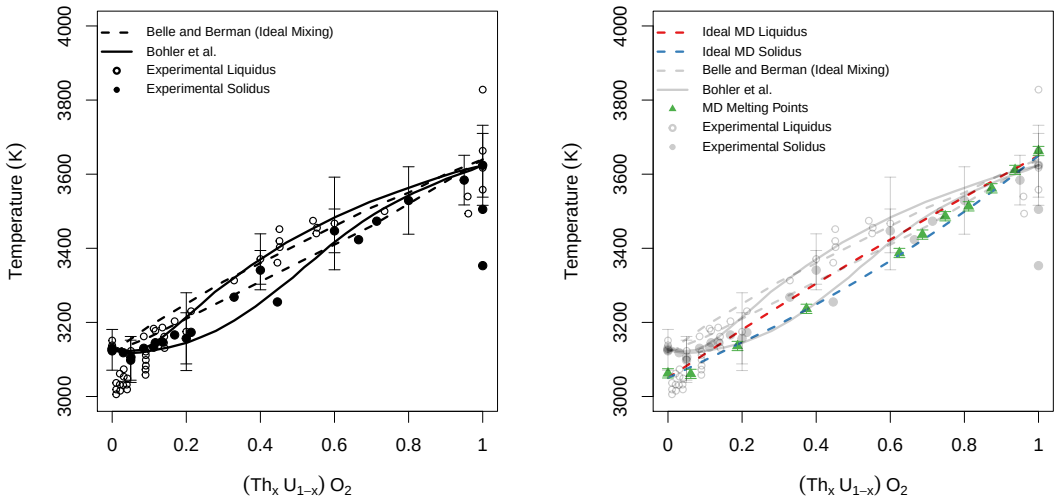

Figure 3: (a) collated experimental $(Th,U)O_2$ binary phase diagram [20, 37, 41, 43, 44]. (b) The experimental data (transparent) and the MD melting points calculated using the moving interface method (green points). The error-bars on the MD melting points (green points) is the range where melting occurs (i.e. the minimum and maximum refer a simulation that did not and did melt, respectively). The red and blue solid lines correspond to the ideal liquidus and solidus using MD input parameters.

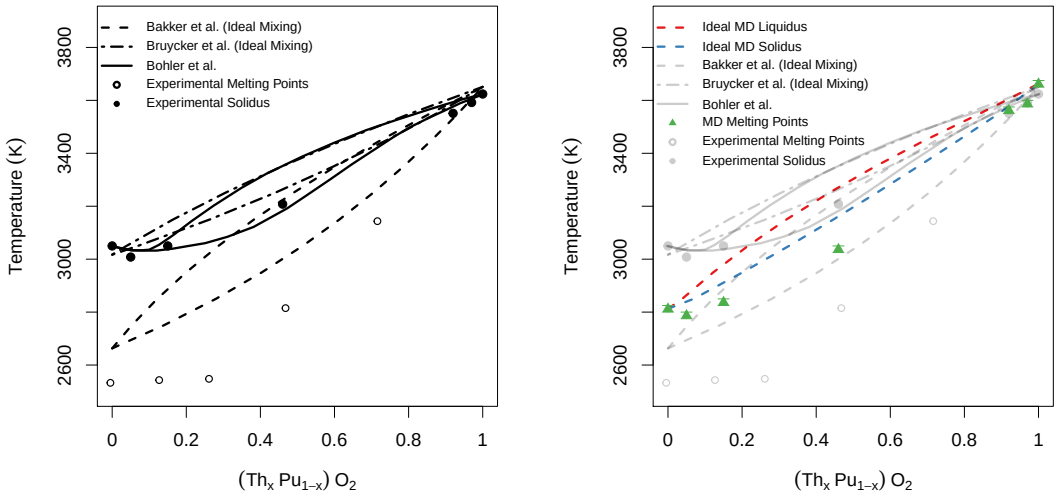

Figure 4: (a) collated experimental $(Th,Pu)O_2$ binary phase diagram [20, 37, 41, 43, 44]. (b) The experimental data (transparent) and the MD melting points calculated using the moving interface method (green points). The error-bars on the MD melting points (green points) is the range where melting occurs (i.e. the minimum and maximum refer a simulation that did not and did melt, respectively). The red and blue solid lines correspond to the ideal liquidus and solidus using MD input parameters.

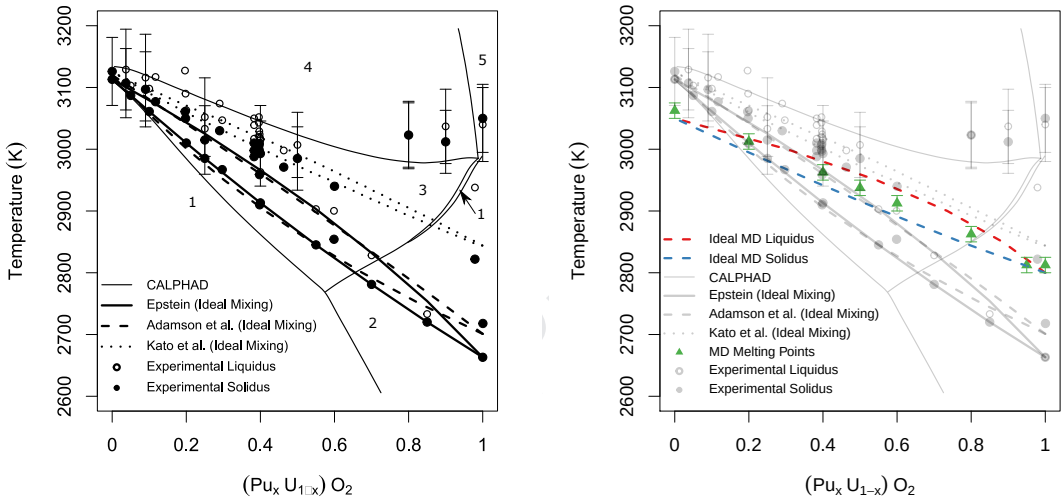

Figure 5: (a) collated experimental (U,Pu)O_2 binary phase diagram [6, 20, 37, 41, 43, 44]. The labels 1,2,3,4 and 5 refer to the solid, solid/gas, solid/liquid, liquid and liquid/gas phases calculated by CALPHAD [6]. (b) The experimental data (transparent) and the MD melting points calculated using the moving interface method (green points). The error-bars on the MD melting points (green points) is the range where melting occurs (i.e. the minimum and maximum refer a simulation that did not and did melt, respectively). The red and blue solid lines correspond to the ideal liquidus and solidus using MD input parameters.

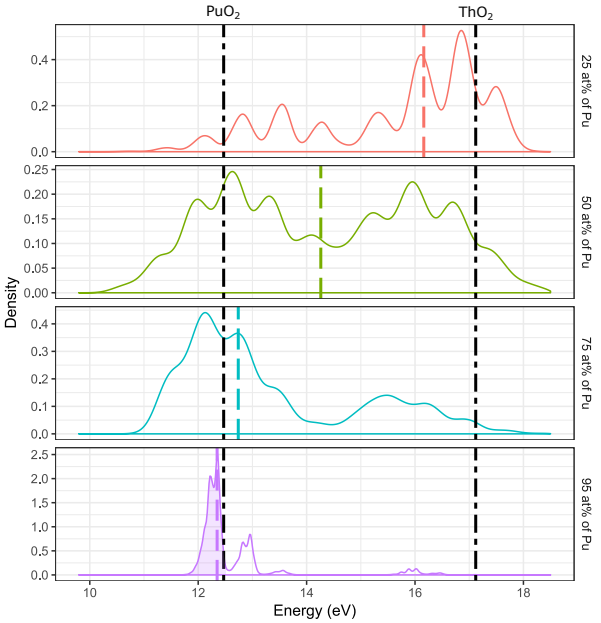

Figure 6: Density of isolated Frenkel energies for $(Pu, Th)O_2$. The black lines are the Frenkel energies for PuO_2 (12.47 eV) and ThO_2 (17.12 eV), respectively. No smoothing was applied. The median values for 25%, 50% and 75% and 95% addition of Pu to ThO_2 are shown by coloured dashed lines (16.2 eV, 14.3 eV, 12.7 eV, 12.3 eV). Note the y-axis have different scales.

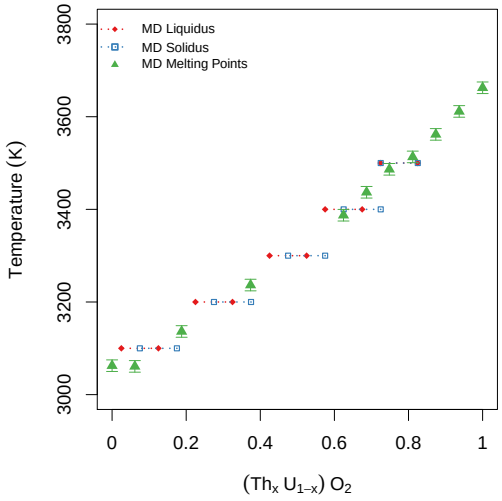

Figure 7: $(Th, U)O_2$ phase diagram where the MD melting points calculated using the moving interface method are shown in green. The error-bars on the MD melting points (green points) is the range in which the system melted (i.e. the minimum and maximum refer to where the simulation did not and did melt, respectively). The red (blue) dots and lines correspond to the uncertainty range over which composition of the liquidus (solidus) can occur, calculated using the CMI method.

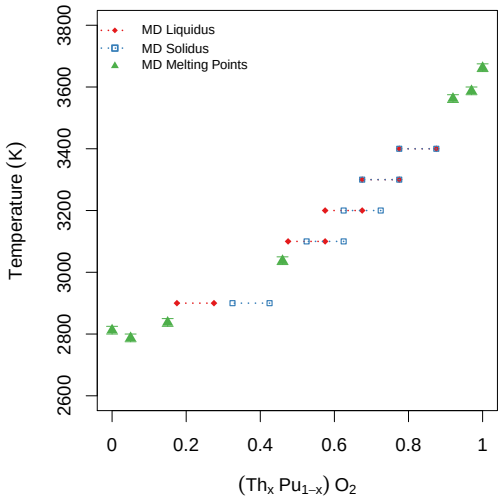

Figure 8: $(Th, Pu)O_2$ phase diagram where the MD melting points calculated using the moving interface method are shown in green. The error-bars on the MD melting points (green points) is the range in which the system melted (i.e. the minimum and maximum refer to where the simulation did not and did melt, respectively). The red (blue) dots and lines correspond to the uncertainty range over which composition of the liquidus (solidus) can occur, calculated using the CMI method.

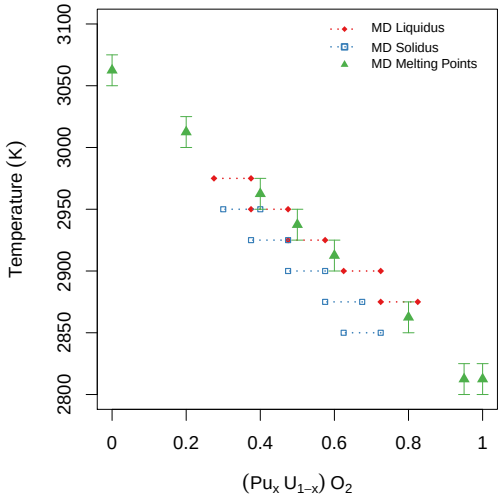

Figure 9: $(Pu, U)O_2$ phase diagram where the MD melting points calculated using the moving interface method are shown in green. The error-bars on the MD melting points (green points) is the range in which the system melted (i.e. the minimum and maximum refer to where the simulation did not and did melt, respectively). The red (blue) dots and lines correspond to the uncertainty range over which composition of the liquidus (solidus) can occur, calculated using the CMI method.

Declaration of interests

☒ The authors declare that they have no known competing financial interests or personal relationships that could have appeared to influence the work reported in this paper.

☐The authors declare the following financial interests/personal relationships which may be considered as potential competing interests: